Journal of Power Sources 185 (2008) 1147–1153

Contents lists available at ScienceDirect

Journal of Power Sources

journal homepage: www.elsevier.com/locate/jpowsour

Liquid water transport between graphite paper and a solid surface

A. Bazylak*, J. Heinrich, N. Djilali, D. Sinton

Department of Mechanical Engineering, and the Institute for Integrated Energy Systems, University of Victoria, Victoria, BC, Canada V8W 3P6

ARTICLE INFO

Article history:
Received 6 June 2008
Received in revised form 9 July 2008
Accepted 9 July 2008
Available online 25 July 2008

Keywords:
Polymer electrolyte membrane fuel cell
Droplet behaviour
Gas diffusion layer
Water management
Gas channel land area
Hydrophobic
Hydrophilic

ABSTRACT

We studied the interaction of a water droplet with a solid wall on a hydrophobic gas diffusion layer (GDL). Of particular interest is the stability of the droplet as a function of plate wetting properties and the potential for liquid entrapment in the GDL/land contact area. Such transport is of relevance to breakthrough dynamics and convective liquid droplet transport in polymer electrolyte membrane (PEM) fuel cell cathode gas channels. While a variety of complex coupled transport phenomena are present in the PEM fuel cell gas channel, we utilize a very simplified experimental model of the system where a droplet originally placed on a hydrophobic GDL is translated quasistatically across the GDL surface by a solid surface. Transport and entrapment are imaged using fluorescence microscopy. This work provides new insights into droplet behaviour at the GDL/land interface in a PEM fuel cell and suggests that hydrophobic land areas are preferable for mitigating the accumulation of liquid water under the land area of the gas flow channels.

1. Introduction

From a surface science perspective, liquid water transport at the interface between a rough porous hydrophobic material in contact with a smooth surface is uncommon; however, such a situation is of particular interest to polymer electrolyte fuel cells [1]. The successful operation of a polymer electrolyte membrane (PEM) fuel cell strongly depends on effective water management [1–3]. Liquid water flooding is still a major hindrance to fuel cell operation at the upper power limits, as excess liquid water hinders reactant gases from reaching the catalyst sites, and flooded gas channels result in parasitic pressure losses. In recent years there have been a number of experimental and numerical investigations to study the spatial distribution of liquid water in PEM fuel cells [4–11], in the gas channels [1,12–20], and in the gas diffusion layer (GDL) [21,22]. Recent efforts to actively remove water in the fuel cell through the use of transport plates [23] and electro-osmotic water pumping [24,25] have also been reported. However investigations have not been published on the effect of the hydrophilic/hydrophobic properties of the gas channel land area on water transport.

Liquid water behaviour under the land area in a PEM fuel cell is a difficult phenomenon to study using *in situ* visualization techniques. In direct optical microscopy, water accumulation under the land area is not visible due to the opaque nature of graphite or metallic plates. However, the tendency for liquid water to accumulate under the land areas of the current collecting plate in PEM fuel cells has been well documented with the use of neutron imaging [5,7] and synchrotron X-ray radiography [11]. In neutron imaging, liquid water can be detected through gold-plated aluminum current collector plates due to the strong interaction between neutrons and hydrogen. A 3–7 μm resolution has been demonstrated with synchrotron X-ray radiography [11], whereas a 25 μm resolution has been demonstrated with neutron imaging [26].

Pekula et al. [5] employed neutron imaging to visualize two-phase flow in an operating PEM fuel cell. At high current densities they observed the accumulation of liquid water under and adjacent to channel walls, particularly at the channel bends. The authors proposed that this accumulation of water could be due to localized pressure variations in the channel or decreased gas flow velocities. Turhan et al. [7] also reported the tendency of liquid water to accumulate under the channel land area in the PEM fuel cell visualized with neutron imaging. Both Pekula et al. [5] and Turhan et al. [7] utilized gold-coated aluminum bipolar plates. Manke et al. [11] employed X-ray radiography to visualize water transport in a PEM fuel cell with graphite bipolar plates, and they also observed the tendency for liquid water to accumulate under the land areas.

PEM fuel cell bipolar plates must exhibit several important qualities. They must exhibit high electrical conductivity to provide efficient electron paths from the gas diffusion media to adjacent cells. Furthermore, bipolar plates must also be impermeable to gas

* Corresponding author. Current Address: Department of Mechanical & Industrial Engineering, University of Toronto, 5 King's College Road, Toronto, ON, Canada M5S 3G8. Tel: +1 416 946 5031; fax: +1 416 978 7753.
E-mail address: abazylak@mie.utoronto.ca (A. Bazylak).

0378-7753/$ – see front matter © 2008 Elsevier B.V. All rights reserved.
doi:10.1016/j.jpowsour.2008.07.031

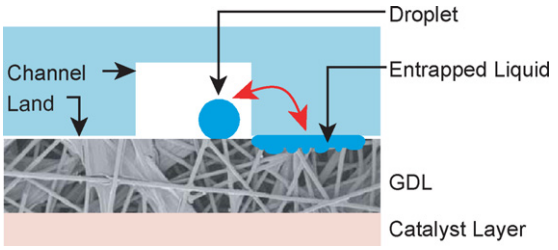

Fig. 1. Schematic of two liquid water transport regimes of interest: stable liquid droplets versus entrapped liquid in the GDL/land area contact region. The contact area between bipolar plate land area and the GDL surface are exaggerated to emphasize the potential for liquid water entrapment.

in order to maintain fuel and oxidant separation [27]. They must exhibit mechanical strength, durability, corrosion resistance, and chemical stability [27,28]. As fuel cell and gas channel dimensions continue to decrease the ease and cost effectiveness of machining or shaping the bipolar plate is becoming increasingly important. Due to the high cost and brittle nature of graphite plates, alternative materials such as carbon composites, metals and stainless steel have been investigated [27]. While these aforementioned qualities are at the forefront of bipolar plate design, there is a significant lack of literature discussing the effect of the bipolar plate's surface wettability on water management in the PEM fuel cell. For instance, does the degree of hydrophobicity affect the spatial distribution of water on the interface between the GDL and bipolar plate? If so, what surface wettability properties are desirable in the fuel cell? It is well-known that water will tend to spread on a hydrophilic surface and form droplets on a relatively hydrophobic surface; however it is not clear whether water will have a tendency to form films within the interfacial region between a highly rough and non-homogeneous hydrophobic material and a smooth and hydrophilic surface, or tendency to form well-defined droplets immediately outside of this region. The work presented in this manuscript provides insight into this very specific region of the fuel cell.

In this paper, we investigate the behaviour of liquid water at the interface between GDLs and bipolar plate land areas with varying degrees of hydrophobicity. In combination with a highly idealized experimental setup, *ex situ* investigations are employed to gain insight on the tendency for liquid water to accumulate under the bipolar plate land area in relation to the hydrophobicity of the land area. Furthermore, the effect of land area wettability on the spatial distribution of water under the land area will be investigated.

2. Experimental methodology

Liquid water transport at the interface between a rough porous hydrophobic material in contact with a smooth surface is not commonly studied from a surface science perspective; however, this type of interface is of particular relevance to PEM fuel cells. The interface between the channel land area and the gas diffusion media is a complex region. This complex region consists of the gas diffusion media with a three-dimensional array of carbon fibers exhibiting a highly rough and hydrophobic surface, which is in contact with a graphite plate with a comparatively smooth surface of lower contact angle (70–80°) [13]. To gain insight on the wettability effects of water transport in this region, we studied the interaction of a water droplet with a solid wall. Of particular interest is the stability of the droplet as a function of plate wetting properties and the potential for liquid entrapment in the GDL/land contact area. Fig. 1 illustrates the two water transport regimes of interest in the GDL/land area: stable droplet and entrapped liquid. While a variety of complex coupled transport phenomena are present in the PEM fuel cell gas channel, we utilized a very simplified experimental model to capture the interaction of a stable droplet originally sitting on the GDL with a solid wall. In this experiment, a droplet was placed on the surface of a GDL, and a simulated bipolar plate interface (glass slide) propagated toward the droplet quasistatically.

2.1. Apparatus and surface preparation

For the present analysis, a Toray TGP-H-060 non-woven fibrous GDL was employed. The TGP-H-060 GDL exhibited a thickness of 190 μm with a mean pore diameter of 23 μm [2]. To investigate the effect of varying the hydrophobicity of the GDL, Toray GDLs with varying degrees of PTFE treatment were employed (0–20%). A GDL sample was secured to a glass plate, as shown in the magnified apparatus view in Fig. 2. A 1.25 μL droplet of water was placed

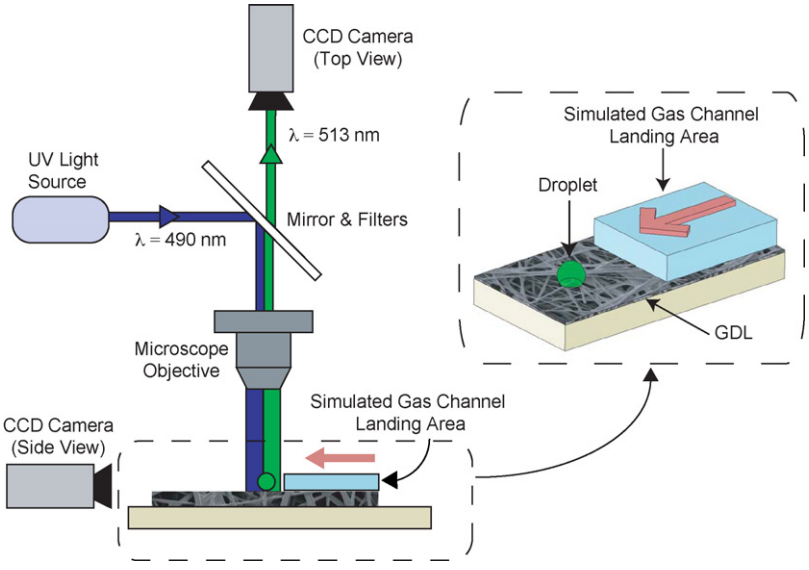

Fig. 2. Schematic of the droplet and land area interaction apparatus with fluorescence microscopy and digital photography arrangement.

on the GDL with a micropipette (Gibson Pipetman P10, 1–10 μL). The droplet size was chosen based on typical droplets observed in minichannels [18]. A solid plate was translated along the surface of the GDL toward the droplet. The plate was connected to a push rod, and plate motion was controlled with a programmable syringe pump (Harvard Apparatus PHD 22/2000). Slow velocities were employed to examine the quasistatic droplet and wall interaction (0.0424 mm s^{-1}). To ensure quasistatic behaviour, the velocity of the plate was decreased by 90%, and the same liquid transport behaviour was observed.

To vary the wettability of the simulated PEM fuel cell land area, three different solid plates were employed: untreated microscope slides, microscope slides with a hydrophobic treatment, and a graphite plate. The plate thickness and static contact angles are summarized in Table 1. The glass slide was a convenient choice of material for simulating the surface properties of the graphite plate commonly employed in PEM fuel cells. Similar to the graphite plate, the glass slide exhibited a highly hydrophilic surface. Further-

Table 1
Solid plate material properties

Plate	Thickness (mm)	Treatment	Contact angle
Esco precleaned microscope slide	1	Untreated	34°
Esco precleaned microscope slide	1	Pennzoil-Quaker State, Rain-X®	101°
Graphite plate	5	Untreated	46°

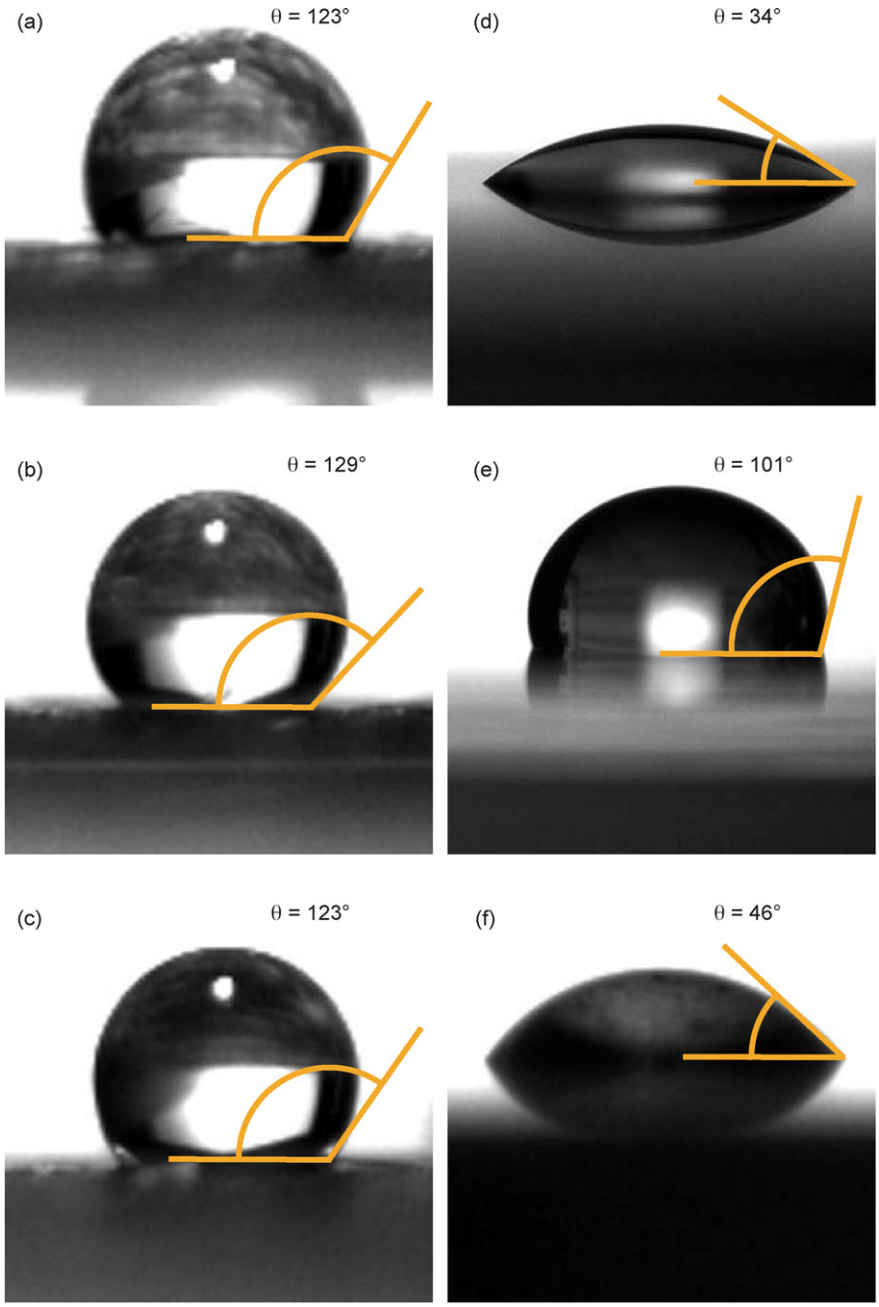

Fig. 3. The contact angle of (a) Toray TGP-H-060 GDL with 0 wt.% PTFE, (b) Toray TGP-H-060 GDL with 10 wt.% PTFE, (c) Toray TGP-H-060 GDL with 20 wt.% PTFE, (d) untreated microscope glass slide, (e) treated microscope glass slide, and (f) graphite plate.

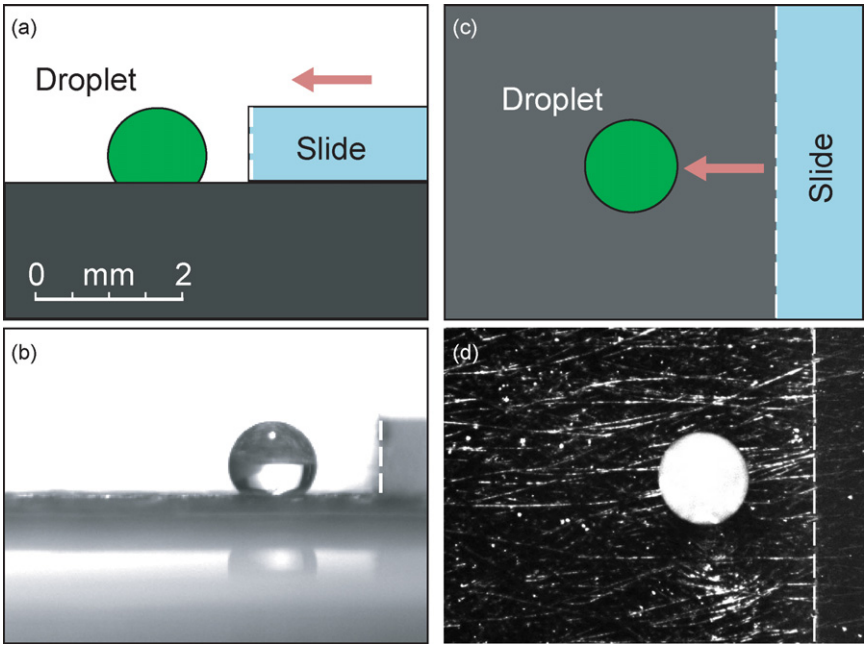

Fig. 4. Schematic illustrating the employed camera position as well as sample captured images: (a) side view of apparatus, (b) sample captured image of the side view, (c) top view of apparatus, and (d) sample fluorescence top view image.

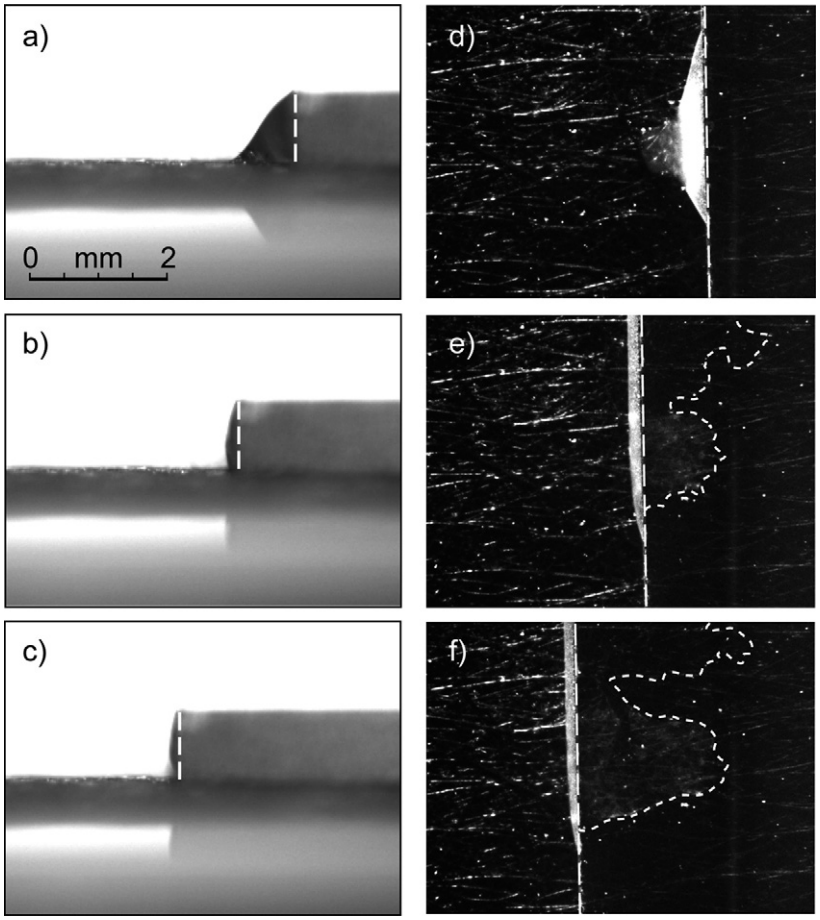

Fig. 5. Images showing the time evolution of a 1.25 μL droplet with a hydrophilic glass slide moving from right to left on a Toray TGP-H-060 10 wt.% PTFE GDL. The left column contains the side view images, and the right column contains the fluorescence top view images. The vertical dashed line indicates the location of the glass wall. For the top view images, the contact line of the entrapped liquid has been outlined with a dashed line for clarity. The first image corresponds to the initial droplet/wall contact, and subsequent images were obtained after 20.5 s. The side view and top view images correspond to the same time within 0.5 s.

more, the transparency of the glass slide allowed optical access to water transport under the surface of the slide. To investigate the droplet/land area interaction with a hydrophobic plate, the microscope slide was treated with a transparent hydrophobic coating (Pennzoil-Quaker State Canada Company, Rain-X®). To apply the coating as per the manufacturer's directions, the glass slide was immersed in the solution, allowed to dry, and lightly buffed with a cloth (Kimtech Kimwipe). This process was repeated three times to the glass slide in order to obtain a highly hydrophobic surface.

The static contact angles (shown in Fig. 3) were measured for these materials using a software package, ImageJ (Wayne Rasband, National Institutes of Health, USA), with the dropsnake plugin [29]. This software was employed to define the contour of the drop as a B-spline curve, which was extended by mirror symmetry to determine the interfacial contact points. The contact angles for the Toray TGP-H-060 GDL did not vary significantly for varying hydrophobic PTFE treatments, as shown in Fig. 3(a) 0 wt.% PTFE, (b) 10 wt.% PTFE, and (c) 20 wt.% PTFE. This is attributed to the non-homogeneous PTFE coverage resulting from the bulk hydrophobic treatment of the GDLs [2]. In contrast, the measured contact angles for the simulated bipolar plate interfaces varied significantly. An untreated glass slide exhibited a contact angle of 34° (Fig. 3(d)), while a treated glass slide became hydrophobic with a contact angle of 101° (Fig. 3(e)). With a contact angle of 46° (Fig. 3(f)), the graphite plate exhibited a similar degree of hydrophilicity to the untreated glass slide.

The apparatus was mounted on a microscope stage (Leica Microsystems DM LM), and the droplet/land area interaction was captured with fluorescence microscopy combined with two cooled CCD cameras. A dilute solution of fluorescein dye (83 ppm, 1 mM) was employed as a tracer for liquid water. In fluorescence microscopy, fluorescein molecules (MW 332.31) are illuminated with blue light (490 nm). The molecules absorb and dissipate the energy with an emission of green light (513 nm). Filters in the optical microscope allowed the green light to reach the vertical mounted CCD camera (Hamamatsu ORCA-AG, 12 bits). The top view images were captured at a frame rate of 1.97 frames s^{-1} and resolution of 1344 pixels × 1024 pixels (0.122 pixels μm^{-1}). Side view images were captured using a cooled CCD camera (QImaging Retiga 1300i Mono, 12 bits) at a frame rate of 2.91 frames s^{-1} and a spatial resolution of 650 pixels × 515 pixels (0.0493 pixels μm^{-1}). Fig. 4 is a schematic illustrating the two types of images presented in this work. Fig. 4(a) is a schematic showing the side view of the apparatus, and Fig. 4(b) is a sample captured image of the side view. Similarly, Fig. 4(c) is a schematic showing the top view of the apparatus, and Fig. 4(d) is a sample captured top view image.

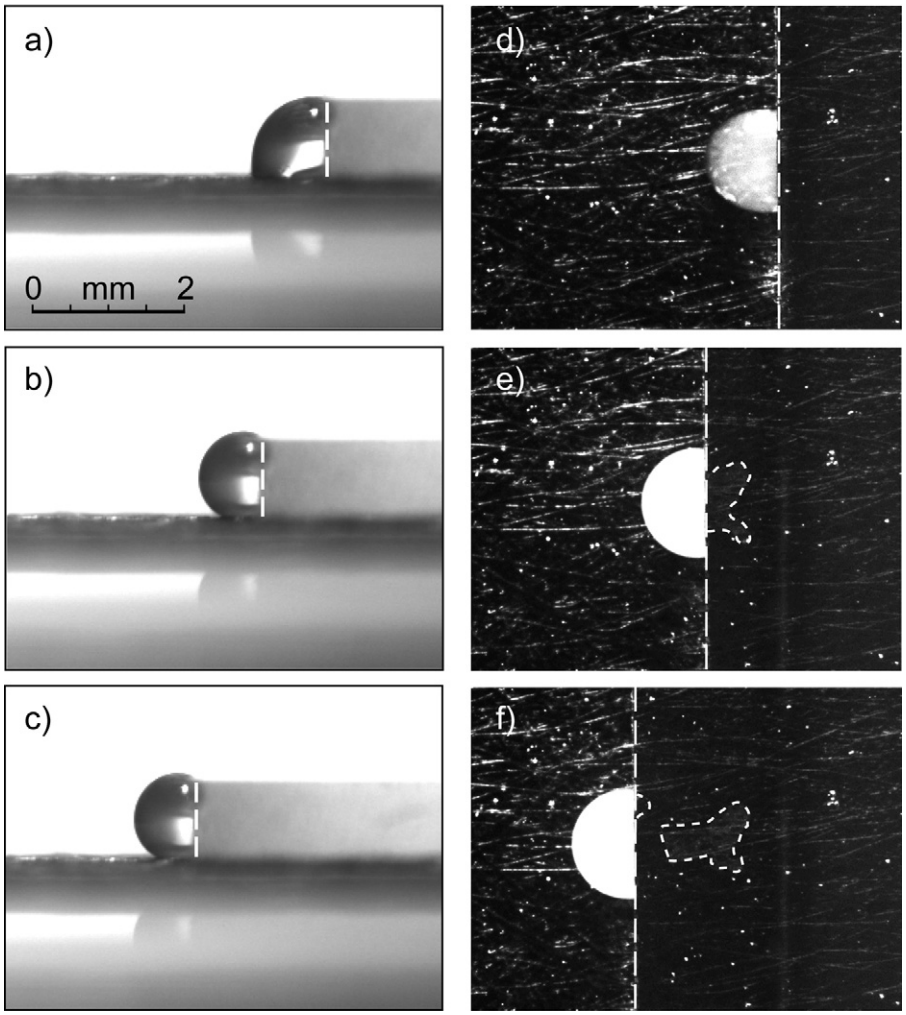

Fig. 6. Images showing the time evolution of a 1.25 μL droplet with a hydrophobic glass slide moving from right to left on a Toray TGP-H-060 10 wt.% PTFE GDL. The left column contains the side view images, and the right column contains the fluorescence top view images. The vertical dashed line indicates the location of the glass wall. For the top view images, the contact line of the entrapped liquid has been outlined with a dashed line for clarity. The first image corresponds to the initial droplet/wall contact, and subsequent images were obtained after 20.5 s. The side view and top view images correspond to the same time within 0.5 s.

3. Results

The quasistatic interaction between a microdroplet and a simulated gas channel land area was investigated with GDLs of varying PTFE treatment combined with hydrophilic and hydrophobic glass slides. Fig. 5 shows the time series evolution of a droplet sitting on a Toray TGP-H-060 10 wt.% PTFE GDL and coming into contact with a hydrophilic glass slide moving quasistatically from right to left. The side view is presented along the left column, while the top view is presented along the right column, and each side and top view image corresponds to the same moment within ±0.5 s. The first images (Fig. 5(a) and (d)) correspond to the initial contact between the stationary droplet and the moving glass slide. The following images (placed below sequentially) are separated by a time period of 20.5 s. The vertical dashed lines indicate the location of the glass wall, and in the top view images, a dashed line indicates the liquid water contact line beneath the glass slide. When the glass wall initially contacted the droplet, the droplet quickly adhered to the hydrophilic surface, spreading along the glass wall as shown in Fig. 5(d). As the glass wall continued to translate along the GDL surface, liquid water became entrapped under the glass surface, as indicated by the dashed lines in Fig. 5(e) and (f). As the liquid becomes entrapped between the GDL and land area, the contact line of the droplet on the wall also continued to spread.

The effect of interchanging the hydrophilic glass slide with a hydrophobic glass slide is shown in Fig. 6. When the hydrophobic glass wall initially contacted the droplet, the movement of the droplet's contact line was minimal, compared to the major readjustment of the contact line observed in Fig. 5(a) and (d) for a hydrophilic glass wall. With a hydrophobic glass wall, the droplet maintained a relatively spherical shape after the initial contact. As the glass wall continued to translate across the GDL, the droplet continued to maintain a spherical shape, as shown in Fig. 6(b) and (c). When comparing Fig. 6(a) with (b) and (c), it can be seen that the contact angle increased as the droplet was pushed by the glass slide. Since the glass slide and GDL were both hydrophobic in this case, water entrapment under the glass slide would not be expected in the absence of pinning. However, small patches were observed (Fig. 6(e) and (f)), and can be accounted for by the presence of pinning due to contact angle hysteresis. Contact angle hysteresis on the surface of the GDL can be accounted for by a non-homogeneous treatment of PTFE along the highly rough and porous surface of the GDL. GDL materials are typically treated in bulk, and thus the PTFE treatment is characterized by an average weight of applied coating. Although a uniform treatment is desired, the resulting GDL is

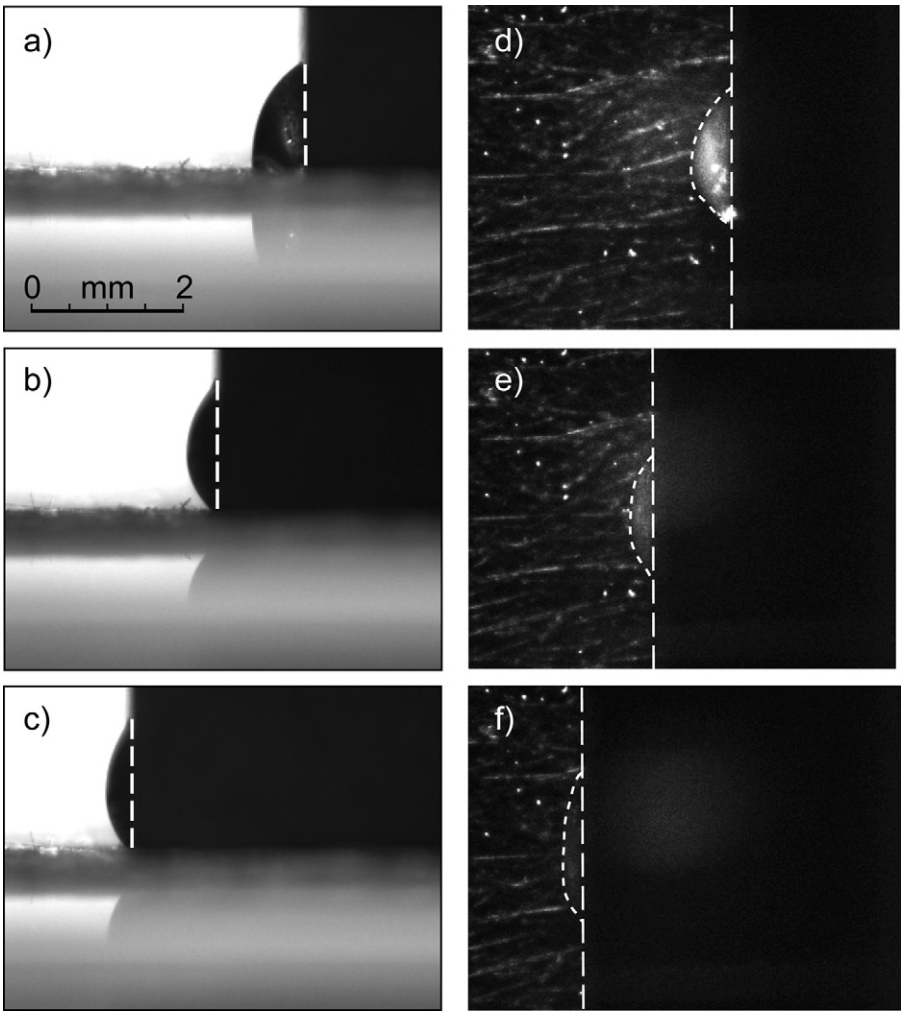

Fig. 7. Images showing the time evolution of a 1.25 μL droplet with a graphite plate moving from right to left on a Toray TGP-H-060 10 wt.% PTFE GDL. The left column contains the side view images, and the right column contains the fluorescence top view images. The vertical dashed line indicates the location of the graphite wall. The first image corresponds to the initial droplet/wall contact, and subsequent images were obtained after 20.5 s. The side view and top view images correspond to the same time within 0.5 s.

typically treated non-uniformly, and the degree of non-uniformity depends on the method of application [2].

Next, the hydrophobic glass slide was replaced with a graphite plate, which resembles the material commonly used for PEM fuel cell bipolar plates. Fig. 7 shows the time series evolution of a droplet interacting with the graphite plate and GDL. When the graphite wall initially contacted the droplet, the droplet underwent a contact line readjustment that was less drastic than for the case of a hydrophilic glass slide, but more so than the hydrophobic glass slide, as expected from the measured contact angles (Table 1). As shown in Fig. 7(a) and (d), the droplet lost its original spherical shape and spread along the graphite wall. As the graphite wall continued to translate across the GDL, the droplet continued to spread. Although the opaque graphite plate prevented the real-time detection of water entrapment under the land area, the presence of the entirely entrapped droplet was confirmed at the end of the trial when the graphite plate was lifted from the GDL sample.

Droplet/land area interaction was also tested for Toray GDLs with 0 and 20 wt.% PTFE, with the same simulated channel land surfaces (hydrophilic glass, hydrophobic glass, and graphite). However, it was found that the level of PTFE treatment did not have a detectable affect on the behaviour of the droplet at the wall, but rather the dominating factor to whether the droplet favoured entrapment was the hydrophobicity of the channel land area. With a hydrophilic land area, the droplets favoured entrapment under the land area, while the opposite was true with a hydrophobic land area.

With respect to experimental error, the trends observed in these experiments were reproducible. However, the precise shape of the wetting patterns varied from case to case. Due to the three-dimensional random nature of the porous material employed, the moving block experiment was a simplified experimental system that enabled the observation of liquid water transport at the interface of a hydrophobic GDL and a solid block. While exact wetting patterns cannot be directly interpreted in the context of water transport in fuel cells, the results indicate that the hydrophobicity of the surfaces does play a significant role in transport at the boundary.

4. Conclusions

The interaction of a water droplet with a solid wall on a hydrophobic GDL surface was investigated. A simplified experimental model of a PEM fuel cell gas channel was employed to study the stability of the droplet as a function of plate wetting properties and the potential for liquid entrapment in the GDL/land contact area. This transport is of relevance to breakthrough dynamics and convective liquid droplet transport in PEM fuel cell cathode gas channels. Single droplets originally placed on a hydrophobic GDL were translated quasistatically across the GDL surface by a solid surface representing the land area in a PEM fuel cell. The side and top view images were captured concurrently through the use of fluorescence microscopy and digital photography. The degree of GDL PTFE treatment had no noticeable effect on the behaviour of the droplet at the wall. The degree of land area hydrophobicity was found to strongly affect droplet behaviour. With a hydrophilic solid surface, the droplet immediately spread and favoured entrapment between the GDL/land area interface. With a hydrophobic solid surface, droplets experienced minimal entrapment. This work presents insight into the gas channel wettability effects on water distribution in a PEM fuel cell. These results indicate that hydrophilic land areas may be beneficial to increase the likelihood of GDL/land area entrapment, whereas if water removal through gas flow is preferred, then hydrophobic gas channels may enhance droplet formation and detachment.

Acknowledgments

The authors are grateful for the financial support of the Natural Sciences and Engineering Research Council (NSERC) of Canada, the Canada Research Chairs Program, and the National Research Council (NRC). The authors would also like to acknowledge the support of the Canadian Foundation for Innovation (CFI).

References

[1] A. Theodorakakos, T. Ous, M. Gavaises, J. Nouri, N. Nikolopoulos, H. Yanagihara, Journal of Colloid and Interface Science 300 (2006) 673–687.
[2] M. Mathias, J. Roth, J. Fleming, W. Lehnert, Handbook of Fuel Cells, John Wiley & Sons, Ltd., New York, 2003, pp. 1–21.
[3] H. Meng, C.-Y. Wang, Journal of The Electrochemical Society 152 (9) (2005) A1733–A1741.
[4] R. Satija, D. Jacobson, M. Arif, S. Werner, Journal of Power Sources 129 (2004) 238–245.
[5] N. Pekula, K. Heller, P. Chuang, A. Turhan, M. Mench, J. Brenizer, K. Unlu, Nuclear Instruments and Methods in Physics Research A 542 (2005) 134–141.
[6] D. Kramer, J. Zhang, R. Shimoi, E. Lehmann, A. Wokaun, K. Shinohara, G. Scherer, Electrochimica Acta 50 (2005) 2603–2614.
[7] A. Turhan, K. Heller, J. Brenizer, M. Mench, Journal of Power Sources 160 (2006) 1195–1203.
[8] T. Trabold, J. Owejan, D. Jacobson, M. Arif, P. Huffman, International Journal of Heat and Mass Transfer 49 (2006) 4712–4720.
[9] J. Owejan, T. Trabold, D. Jacobson, D. Baker, D. Hussey, M. Arif, International Journal of Heat and Mass Transfer 49 (2006) 4721–4731.
[10] J. Zhang, D. Kramer, R. Shimoi, Y. Ono, E. Lehmann, A. Wokaun, K. Shinohara, G. Scherer, Electrochimica Acta 51 (2006) 2715–2727.
[11] I. Manke, C. Hartnig, M. Grünerbel, W. Lehnert, K. Kardjilov, A. Haibel, A. Hilger, J. Banhart, H. Riesemeier, Applied Physics Letters 90 (2007), 174105-1–174105-3.
[12] K. Tüber, D. Pcza, C. Hebling, Journal of Power Sources 124 (2003) 403–414.
[13] X. Yang, F. Zhang, A. Lubawy, C.-Y. Wang, Electrochemical and Solid-State Letters 7 (11) (2004) A408–A411.
[14] A. Hakenjos, H. Muenter, U. Wittstadt, C. Hebling, Journal of Power Sources 131 (2004) 213–216.
[15] K. Sugiura, M. Nakata, T. Yodo, Y. Nishiguchi, M. Yamauchi, Y. Itoh, Journal of Power Sources 145 (2005) 526–533.
[16] J. Borrelli, S. Kandlikar, T. Trabold, J. Owejan, (ICMM2005-75118) Proceedings of the 3rd International Conference on Microchannels and Minichannels, June 13–15, 2005.
[17] J. Kowal, A. Turhan, K. Heller, J. Brenizer, M. Mench, Journal of the Electrochemical Society 153 (10) (2006) A1971-–A1978.
[18] E. Kumbur, K. Sharp, M. Mench, Journal of Power Sources 161 (2006) 333–345.
[19] F.-B. Weng, A. Su, C.-Y. Hsu, C.-Y. Lee, Journal of Power Sources 157 (2006) 674–680.
[20] D. Spernjak, A. Prasad, S. Advani, Journal of Power Sources 170 (2007) 334–344.
[21] S. Litster, D. Sinton, N. Djilali, Journal of Power Sources 154 (2006) 95–105.
[22] A. Bazylak, D. Sinton, Z.-S. Liu, N. Djilali, Journal of Power Sources 163 (2007) 784–792.
[23] A.Z. Weber, R.M. Darling, Journal of Power Sources 168 (2007) 191–199.
[24] C.R. Buie, J.D. Posner, T. Fabian, S.-W. Cha, D. Kim, F.B. Prinz, J.K. Eaton, J.G. Santiago, Journal of Power Sources 161 (2006) 191–202.
[25] S. Litster, C.R. Buie, T. Fabian, J.K. Eaton, J.G. Santiago, Journal of The Electrochemical Society 154 (10) (2007) B1049-–B1058.
[26] D. Hussey, D. Jacobson, M. Arif, J. Owejan, J. Gagliardo, T. Trabold, Journal of Power Sources 172 (2007) 225–228.
[27] H. Wang, M. Sweikart, J. Turner, Journal of Power Sources 115 (2003) 243–251.
[28] B. Cunningham, D. Baird, Journal of Power Sources 168 (2007) 418–425.
[29] A. Stalder, G. Kulik, D. Sage, L. Barbieri, P. Hoffmann, Colloids and Surfaces A: Physicochemical and Engineering Aspects 286 (1–3) (2006) 92–103.